Synthesis and Characterization of Polymethacrylates Containing Conjugated Oligo(phenylene ethynylene)s as Side Chains

Alexander M. Breul,[1,2] Johann Schäfer,[2,3] Georgy M. Pavlov,[1,2] Anke Teichler,[1,2,4] Stephanie Höppener,[1,2,4] Christine Weber,[1,2,4] Jürgen Nowotny,[1,2] Lars Blankenburg,[5] Jürgen Popp,[2,3,6] Martin D. Hager,[1,2,4] Benjamin Dietzek,[2,3,6] Ulrich S. Schubert[1,2,4]

[1]Laboratory of Organic and Macromolecular Chemistry (IOMC), Friedrich-Schiller-University Jena, Humboldtstr. 10, 07743 Jena, Germany
[2]Jena Center for Soft Matter (JCSM), Friedrich-Schiller-University Jena, Humboldtstr. 10, 07743 Jena, Germany
[3]Institute of Photonic Technology Jena e.V. (IPHT), Albert-Einstein-Straße 9, 07745 Jena, Germany
[4]Dutch Polymer Institute (DPI), P.O. Box 902, 5600 AX Eindhoven, The Netherlands
[5]Thüringisches Institut für Textil- und Kunststoff-Forschung e.V. (TITK), Breitscheidstr. 97, D-07407 Rudolstadt, Germany
[6]Institute of Physical Chemistry (IPC) and Abbe Center of Photonics (ACP), Friedrich-Schiller-University Jena, Helmholtzweg 4, 07743 Jena, Germany
Correspondence to: M. D. Hager (E-mail: martin.hager@uni-jena.de) or B. Dietzek (E-mail: benjamin.dietzek@uni-jena.de) or U. S. Schubert (E-mail: ulrich.schubert@uni-jena.de)

Received 28 March 2012; accepted 4 April 2012; published online 17 May 2012
DOI: 10.1002/pola.26105

ABSTRACT: In order to form suitable systems designed for resonance energy transfer, a series of monodisperse methacrylate-based monomers containing rigid π-conjugated oligo(phenylene ethynylenes) with different sizes of the conjugated systems (**M1**–**M3**), and therefore different optoelectronic properties, were synthesized and subsequently polymerized using the reversible addition–fragmentation chain transfer polymerization technique (**P1**–**P3**). In addition, these oligomers were also copolymerized with methyl methacrylate. The obtained polymers were characterized by ^{1}H NMR spectroscopy, size exclusion chromatography, and analytical ultracentrifugation. The photophysical properties of the polymers were studied by UV–vis absorption and emission spectroscopy in diluted solutions as well as in thin films and compared to the photophysics of the corresponding monomers. Thereby, changes going from monomeric to polymeric systems could be detected in fluorescence quantum yields and lifetimes pointing to energy trapping, e.g., energy transfer. Donor–acceptor copolymers containing different numbers of monomeric units within the side chain exhibit differences in the emission spectra, indicating that energy trapping in polymers is very sensitive to structural properties such as the chain length. UV–vis absorption spectroscopy as well as time-resolved lifetime studies indicate intrapolymer and interpolymer energy transfer. © 2012 Wiley Periodicals, Inc. J Polym Sci Part A: Polym Chem 50: 3192–3205, 2012

KEYWORDS: dyes/pigments; energy transfer; fluorescence; monodisperse oligo(phenylene ethynylene)s; reversible addition fragmentation chain transfer polymerization (RAFT); π-stacking

INTRODUCTION During the past decade, the field of comb polymers attracted significant attention in various areas, e.g., (hybrid) nanostructures,[1–4] biomedicine,[5–7] super soft elastomers,[8,9] photonics,[10] and thermoresponsive polymers with lower critical solution temperature behavior.[11–13] The dense packing of the side chains covalently bound to a linear backbone causes confined and compact structures, in particular, worm-like conformations.[14] Hence, notable chain end effects can be observed. The incorporation/attachment of conjugated oligomers to nonconjugated backbones leads to a variety of different structures due to the wide range of possible pendant molecules revealing chemical stability, photoconductivity of the attached π-electron systems, and an invariance of the standard oxidation/reduction potential with the degree of substitution.[15] In order to take advantage of these possibilities, conjugated oligomers were attached either to aliphatic polymers as side chains or in dendritic structures.[16] The resulting polymers combine the typical polymer properties (e.g., film forming ability, mechanical stability, and processing advantages)[16] with the well-defined electronic, photonic, and morphological properties of the monodisperse oligomer moieties. In addition, the generally low solubility of

Alexander Breul and Johann Schäfer equally contributed to this work.
Additional Supporting Information may be found in the online version of this article.

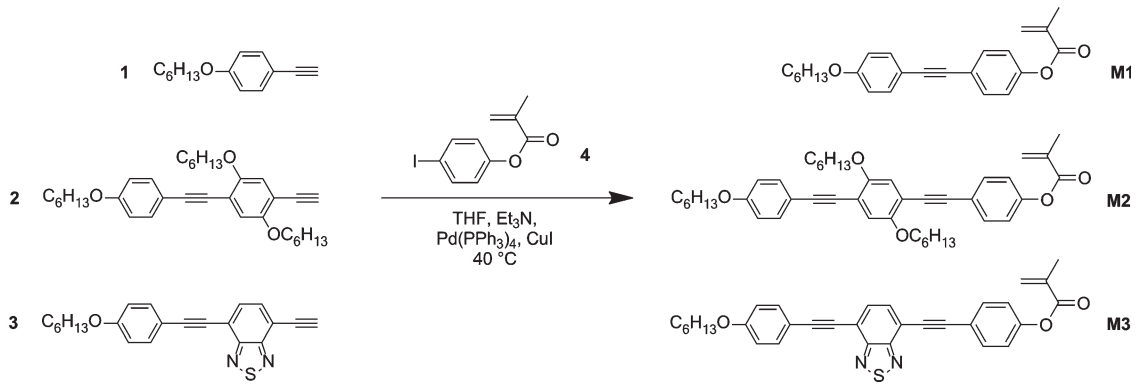

SCHEME 1 Schematic representation of the monomer synthesis.

the oligomers can be improved significantly. For this purpose, a large variety of π-conjugated oligomers – for instance, carbazoles,[17] triphenylamines,[15] perylenes,[18] diphenylacetylene units,[19] and oligothiophenes[20] – were attached to aliphatic backbones (e.g., methacrylates) as side chains. Diverse block copolymers published by Thelakkat and coworkers[21–25] revealed good phase separation behavior featuring nanodomain sizes between 5 and 20 nm. Thus, they became attractive for applying them in bulk hetero-junction organic solar cells. This defined distance lies not only within the range of the exciton diffusion length which plays a significant role for organic photovoltaics but also in the range of the Förster radius of the most suitable dyes for the Förster resonant energy transfer (FRET). So far, the light-harvesting properties of selected dyes, e.g., coumarins[26,27] or 4-hydroxy thiazoles,[28] were used to transfer the energy to Ru(II) trisbipyridine complexes along the polymer chain.

In this contribution, the design and synthesis of new comb polymers with π-conjugated oligomers as side chains are described to combine the well-defined optoelectronic properties of the oligomers with typical processing properties of common polymers. For this purpose, the synthesis of different monomers that consist of a monodisperse oligo(phenylene ethynylene) (OPE) moiety and a methacryl end group as a polymerizable function was targeted (**M1**–**M3**). The rod-like structure of the triple bond results in rigid, linear, and planar oligomers, enabling the possibility for a supramolecular arrangement, e.g., via stapling and π-stacking.[29,30] Subsequently, these monomers were polymerized using a controlled radical polymerization (CRP) technique, specifically the reversible addition–fragmentation chain transfer (RAFT) method.[31] The precisely defined length, conformation, and constitution of the monomers allow a reliable prediction of structure–property relationships.[32] In addition, one can gain further information about the folding properties of the corresponding polymers. The close spatial arrangement of the conjugated oligomers in the polymer chain should lead to increased intermolecular interactions compared with the isolated and independent oligomers. As a consequence, the polymers presented are capable to act as light harvesters possibly for artificial photosynthetic systems, like, hydrogen evolving metal complexes[33–36] or as sensitizers for ruthenium complexes.[28] Similar to the natural light-harvesting units, where fast RET and funneling to a reaction center occurs because of short interchromophore distance and adequate spatial arrangement,[37] the polymers at hand allow for RET and energy funneling from a donor to an acceptor. The Förster radius of 43 Å for the donor–acceptor pair **M2**/**M3** illustrates this potential and is comparable to other tailor-made donor–acceptor pairs.[38] The homopolymers **P2** and **P3** as well as the polymers **P2**-***stat***-**P3** and **P2**-***stat***-**PMMA**-***stat***-**P3** are potentially light-harvesting units for an enhanced excitation of reaction centers by light to use their photosynthetic capacity.

RESULTS AND DISCUSSION

Synthesis

Three monodisperse oligomeric conjugated monomers based on phenylene ethynylene units were synthesized in moderate to good yields by multiple sequential Sonogashira cross-coupling reactions (Scheme 1). The donor monomer **1**, the donor dimer **2**, and the acceptor trimer **3** were coupled with the functional methacrylate **4**. By this manner, the conjugated system was extended and the polymerizable function – i.e., the methacrylate – was introduced. Noteworthy, no side reactions of the double bond or polymerization of the methacrylate occurred during the Sonogashira cross-coupling reaction. Further details are summarized in Supporting Information. The rigid, rod-like character of the monomers is expected to promote π-stacking and ordering by its close spatial arrangement along the polymer chain.

For all polymerizations of the three different monomers **M1**–**M3**, a standard procedure of the RAFT polymerizations technique[39] was applied (Scheme 2, Table 1). In the following paragraphs, the nomenclature for the different substances is applied as follows: the capital letter **M** stands for the monomers, whereas **P** is used for polymers. The monomers and polymers, respectively, were numbered from **1** to **3** in order to demonstrate the type of the conjugated system that is attached to the polymerizable function and backbone, respectively. **1** symbolizes the donor dimer, **2**, donor trimer, and **3**, acceptor trimer. The small indices **a**–**e** indicate the difference of the samples that were synthesized in different

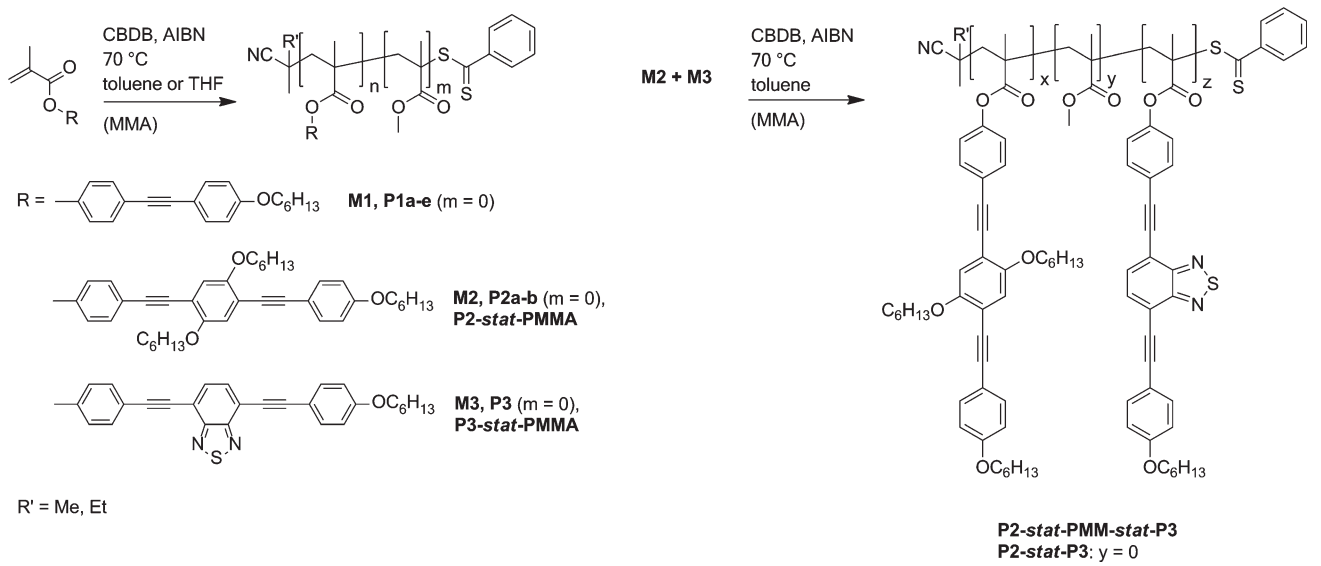

SCHEME 2 Schematic representation of the RAFT polymerization of **M1–M3** (left) and the donor–acceptor copolymers (right).

batches to obtain different molar masses and chain lengths, respectively. Consequently, the statistical donor–acceptor copolymer is abbreviated by **P2-*stat*-P3**. Furthermore, copolymers with an increased distance between the single oligomers were synthesized. For this purpose, the dyes were "diluted" with methyl methacrylate (MMA) as comonomer. In case of these polymers, "**-*stat*-PMMA**" was inserted into the abbreviation. 2,2′-Azo*bis*(*iso*-butyronitrile) (AIBN) was used as an initiator and 2-cyanobutan-2-yl benzodithioate (CBDB) as a chain transfer agent.[13] Generally, toluene was used as solvent, but for the polymerizations of **M3**, tetrahydrofuran (THF) was applied, due to the low solubility of **M3** in toluene. The chain length of the polymers could be adjusted by the variation of the [monomer]:[CBDB] ratio. For the polymerization of the statistical donor–acceptor polymer **P2-*stat*-P3**, a ratio of **M2**:**M3** of 1:1.5 was used. The resulting copolymer had a composition of 30% **M2** and 70% **M3**, which was calculated from the ^{1}H NMR spectrum (Supporting Information) indicating a slightly enhanced incorporation of **M3** into the copolymer. Because of the high molar masses of the monomers (662.9 g/mol for **M2** and 520.6 g/mol for **M3**), the conversions of the monomers could not be determined separately by gas chromatography. Alternatively, size exclusion chromatography (SEC) using a UV-detector could not be used to determine both monomer conversions, because both monomers show equal retention times (no baseline separation) due to the relatively low difference in molar masses compared to the whole calibration range of the SEC column with the lowest exclusion limit. Furthermore, ^{1}H NMR shifts are overlapping for the vinyl as well as for

TABLE 1 Summary of the Observed Molar Masses (M_n, SEC), PDI Values, M/CBDB Ratios, Reaction Times, and Monomer Conversions of all Synthesized Polymers

Sample	M_n, SEC (g/mol)	PDI	M/CBDB	Reaction time (h)	Conversion (%)
P1a	17,000[a]	1.29	60	16	64
P1b	24,000[a]	1.37	60	20	85
P1c	33,100[a]	1.85	60	23	93
P1d	8,800[a]	1.25	20	16	74
P1e	16,400[a]	1.29	60	14	77
P2a	13,600[a]	1.20	60	25	44
P2b	14,400[a]	1.24	20	17	83
P3	11,100[a]	1.20	20	16	87
P2-*stat*-P3	9,300[a]	1.16	20	18	–
P2-*stat*-PMMA	14,600[b]	1.24	100	8.5	64 (MMA), 79 (**M2**)
P3-*stat*-PMMA	10,500[b]	1.17	100	7	66 (MMA), 91 (**M3**)
P2-*stat*-PMMA-*stat*-P3	10,800[b]	1.30	150	16	29 (MMA)

[a] $CHCl_3$, PS standard. [b] $CHCl_3$, PMMA standard.

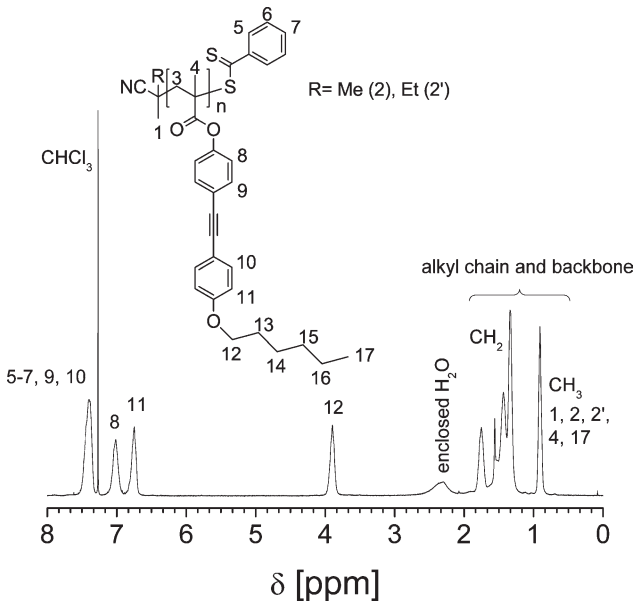

FIGURE 1 ^{1}H NMR spectrum of **P1a** ($CDCl_3$, 300 MHz).

the aromatic proton signals due to their similar surrounding at the polymerizable function; as a consequence, no conversion over time plot could be measured. In this case, **M3** seems to be incorporated slightly faster in the polymeric backbone. Under the same reaction conditions for the polymerizations as already described above, monomer **M3** was also incorporated faster than the MMA in the PMMA-containing copolymer **P3-*stat*-PMMA**. For the polymer **P2-*stat*-PMMA**, an [oligomer]:[MMA] ratio of 1:9 was applied for the polymerization resulting in a donor trimer content of 14%. Having the increased polymerization rate of **M3** in mind, the ratio between of [MMA]:[**M3**] was set to 97:3 for the copolymerization. The obtained content of acceptor trimer in **P3-*stat*-PMMA** was 8%. For the PMMA-containing donor–acceptor copolymer **P2-*stat*-PMMA-*stat*-P3**, a reaction mixture with a [**M2**]:[**M3**]:[**MMA**] ratio of 8:16:76 was used to obtain a comparable donor–acceptor ratio to **P2-*stat*-P3**. The final composition of the polymer reveals 12% donor trimer, 24% acceptor trimer, and 64% PMMA. A potential explanation for the increased oligomer content could be the purging process before the polymerization, due to the evaporation of MMA.

Structural Characterization and Molar Masses

The obtained polymers were characterized by ^{1}H NMR spectroscopy and SEC. The aromatic bands, the alkoxy chains, and the backbone protons can be distinguished for all samples. Fig. 1 provides a representative ^{1}H NMR spectrum of **P1a** (see Supporting Information for **P2**, **P3**, **P2-*stat*-PMMA**, **P3-*stat*-PMMA** as well as **P2-*stat*-P3** and **P2-*stat*-PMMA-*stat*-P3**). The ^{1}H NMR spectrum depicts that the splitting of the monomer signals (for the ^{1}H NMR spectra of the monomers, see the Supporting Information) disappeared after the polymerization and turned into the typical broad polymer signals. The vinylic protons of the methacrylate moiety of the monomer also vanished. Alkyne functions are known to polymerize by free RP[19] and during the nitroxide-mediated polymerization[40] process, whereas they are stable during the RAFT polymerization.[41,42] To prove that the triple bonds stay unaffected during the RAFT polymerization, ^{13}C NMR spectra were recorded. The typical shifts of tertiary carbon signals that belong to alkyne functions are located at around 90 ppm (see Supporting Information for ^{13}C NMR spectrum of **P1d**). Additionally, the solubility did not decrease significantly after the polymerization (bad solubility or swelling is an indication for cross-linking). A further proof for the stability of triple bonds throughout the RAFT process is given in the "optical properties" section below.

Table 1 summarizes the molar masses obtained by SEC, the according polydispersity index (PDI) values, and the monomer conversions of each polymerization. It is possible to obtain well-defined polymers with conjugated side chains which have PDI values between 1.15 and 1.30, as typically obtained for RAFT polymerizations. A control over the reaction could be obtained up to conversions of approximately 90%. For higher conversions, the PDI values increased (**P1c**), which was already described, e.g., for polymerizations of *N*-isopropylacrylamide.[43] This is a well-known phenomenon for CRP due to possible chain coupling reactions that are more likely to occur at higher conversions.[31] The conversions were calculated using ^{1}H NMR spectroscopy. The molar masses, which were obtained by SEC measurements, are based on polystyrene (PS) standards (see Fig. 2 for SEC traces for all **P1** samples; for **P1c**, the exclusion limit of the column was reached). Therefore, the question arises if the molar mass is also overestimated, as in the case of conjugated linear PPEs.[44]

In order to investigate this issue, three selected samples (**P1b**, **P1d**, and **P1e** all with a narrow molar mass distributions) were studied in toluene by analytical ultracentrifugation (AUC) – an absolute molar mass characterization method – to obtain more information about the "real" molar masses of the polymers. The calculation of the average M_n and M_w values by the Svedberg equation is sophisticated and depends on the relation between the sedimentation velocity coefficient and the molar mass. The obtained value $M_{sD} \equiv M_{sf}$ is situated

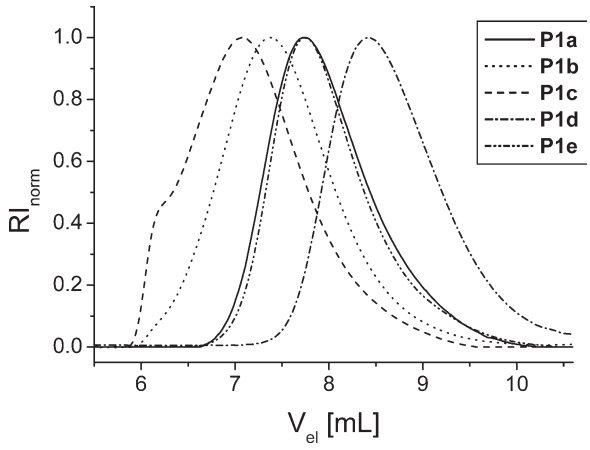

FIGURE 2 SEC traces of **P1a** to **P1e** ($CHCl_3$/isopropyl alcohol/triethylamine).

TABLE 2 Comparison of the Molar Masses Obtained by SEC and AUC

Sample	M_n, SEC[a] (g/mol)	$(M_n + M_w)/2$[b] (g/mol)	M_{AUC} (g/mol)
P1b	24,000	28,400	58,000
P1d	8,800	9,900	14,000
P1e	16,400	18,800	27,000

[a] $CHCl_3$, PS calibration.
[b] M_n and M_w determined by SEC.

between M_n and M_w, in the case of an ideal solvent system $M_{sD} \equiv M_{sf} = (M_n + M_w)/2$. In this case, the situation is close to the "ideal" one (i.e., the thermodynamically ideal solution).

Table 2 compares the molar masses obtained by the two different analytical methods. The problem for the SEC measurements is that there is no comparable standard for the synthesized polymers. In all cases, the PS standard was considered as the best suitable one. The values between SEC and AUC differ by the factor 1.4 up to more than 2. In contrast to linear PPEs, where the molar masses are overestimated by SEC due to the rigid structure,[44] the molar mass of the investigated polymers is underestimated in the SEC measurements. This is supposed to be a result of the dense comb-like structure of the polymers that hinders the formation of loose polymer coils (e.g., as in the case of PS) in solution.[14]

In contrast to the homopolymers **P1**–**P3** and **P2**-***stat***-**P3**, the PMMA-containing copolymer's molar masses were determined only by SEC (Table 1). The accordance between the theoretical molar masses and the measured ones leads to the conclusion that SEC provides reliable values. Furthermore, the low content of oligomers incorporated is expected not to cause significant changes in the hydrodynamic volume of the polymers compared to the PMMA standards.

Optical Properties

The target of this work was the design of new comb polymers with conjugated, monodisperse side chains, and to study the optical behavior of the resulting structures. For that purpose, five different structures have been chosen: the donor–dimer polymers (**P1**), the donor–trimer polymers (**P2**/**P2**-***stat***-**PMMA**), and in contrast to the others, the two electron withdrawing moiety containing acceptor–trimer polymers (**P3**/**P3**-***stat***-**PMMA**). The connection of the side groups by the polymeric backbone is expected to cause a stronger intermolecular and intramolecular packing (π-stacking) as well as ordering of the conjugated oligomers, compared to single oligomers. In contrast to the homopolymers, for the polymers which are not dye-functionalized throughout the whole polymer backbone, this effect is not expected.

Table 3 summarizes selected optical properties of the synthesized monomers and polymers, in particular, absorption and emission maxima and the according extinction coefficients, quantum yields, and lifetimes.

First, the absorption and emission behavior of the monomers and of the according polymers (solutions and films) were compared (Fig. 3 for **M2**/**P2**). It is illustrated that in every case, the polymers showed, as expected, the same absorption in solution compared with their corresponding monomers. The identical absorption and emission behavior of the monomers and polymers are the final proof that the conjugated system of the monomers stays unaffected during the RAFT polymerization process. In the case of alkyne polymerization, a cross-linking would occur which would, as a consequence, lead to an enlargement of the conjugated system. Therefore, additional bands in the UV–visible (UV–vis) absorption and emission spectra would necessarily have to appear.

All polymer films revealed a slight bathochromic shift of 5–10 nm of the absorption maxima. This represents a first indication for interactions of the conjugated side chains in the film.[45] In contrast, the oligomers featured worse or no film formation. A red-shift of the emission maxima of the polymer solutions compared to the monomer solutions as well as a red-shift of the emission maxima of the polymer film compared with polymer solutions was observed in each case. For **P1** and **P2**, this effect is much stronger for the polymer films than for the polymer solutions whereas the formation of the film has no influence on the emission for **P3** (see Supporting Information for selected UV–vis spectra). This means that for **P1** and **P2**, a film formation induces a further planarization and interaction of the oligomers, whereas in the case of **P3**, the side chains might be already aligned planar in solution due to the lower steric hindrance of less alkoxy side chains.[46,47]

Another strong evidence for increased side chain interactions in the polymers is depicted in Fig. 4 for **P2** (see Supporting Information for the spectra of **P1**, **P3** as well as **P2**-***stat***-**P3**). The monomer and the according polymer absorption

TABLE 3 Summary of Selected Optical Properties of the Monomers

Sample	λ_{abs} (nm)	λ_{em} (nm)	ν_{stokes} (cm^{-1})	Φ (%)	τ_1 (ns)	τ_2 (ns)	E_{gap} (eV)
M2	318, 369	402	2, 224	47	0.66		3.08
P2b	313, 369	406	2, 469	22	1.17 (0.33)[a]	0.21 (0.31)[a]	3.08
P2-*stat*-PMMA	317, 369	406	2, 469	67	0.91		3.08[a]
M3	312, 431	529	4, 298	82	5.43		2.58
P3	308, 427	536	4, 762	6	1.48 (0.40)[a]	0.26 (0.35)[a]	2.58
P3-*stat*-PMMA	310, 430	529	4, 352	61	4.11		2.58

[a] In brackets preexponential factors of the double exponential fit are given.

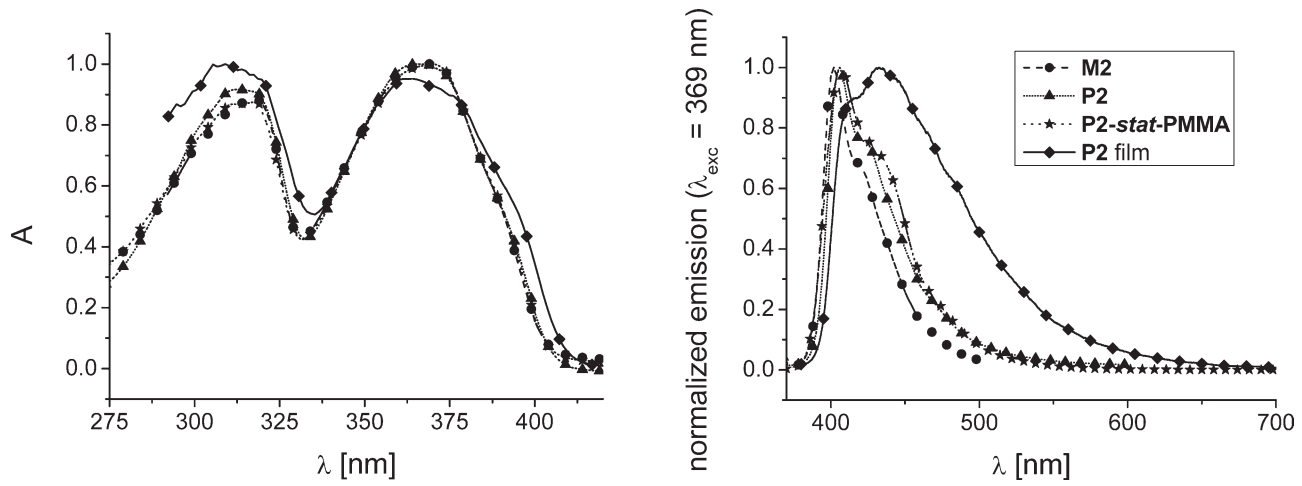

FIGURE 3 UV–vis absorption (left) and emission spectra (right) of **M2** and **P2** in $CHCl_3$ ($c = 10^{-5}$ M).

behavior were studied in $CHCl_3$ solution under increasing MeOH content in solution (vol %). The lower solubility of the polymer in MeOH should force the polymer chains to collapse as well as the side chains to planarize and to interact with increasing MeOH concentration.

In fact, the spectral behavior of all three homopolymers is altered upon MeOH addition, whereas the monomer absorption behavior is independent from the $CHCl_3$:MeOH ratio. For all PMMA-containing polymers, a dependency on the solvent:non-solvent ratio could not be observed. The absorption of the homopolymers was red-shifted and comparable to the polymer film. This effect is stronger for the longer conjugated side chains, due to the lower flexibility and the increased π-conjugated system. First changes occur at MeOH contents between 40 and 50% due to an increasing aggregation.[48] **P2** as well as **P3** could not be measured in solutions with MeOH contents higher than 80 and 60%, respectively, due to the onset of precipitation.

In order to investigate a potential energy transfer from a donor to an acceptor unit within the comb polymes, a statistical copolymer **P2-*stat*-P3** was prepared. For a more facile comparison, an analogous mixture of both homopolymers (30:70 **P2**:**P3**) was investigated via UV–vis spectroscopy in $CHCl_3$ solution with increasing MeOH content (Supporting Information). In both cases, a similar behavior was observed concerning the lowered absorbances as well as the bathochromic shifts of the maxima. In order to investigate the influence of the distance between the donors and acceptors, a PMMA-containing D–A copolymer (**P2-*stat*-PMMA-*stat*-P3**) was prepared. In this case, the PMMA-containing analogous donor and acceptor polymers were used as references. For this purpose, a mixture of **P2-*stat*-PMMA** and **P3-*stat*-PMMA** was prepared with the same donor:acceptor ratio (1:2) as in **P2-*stat*-PMMA-*stat*-P3** and diluted to the same absolute absorbance in solution to ensure a comparable chromophore concentration.

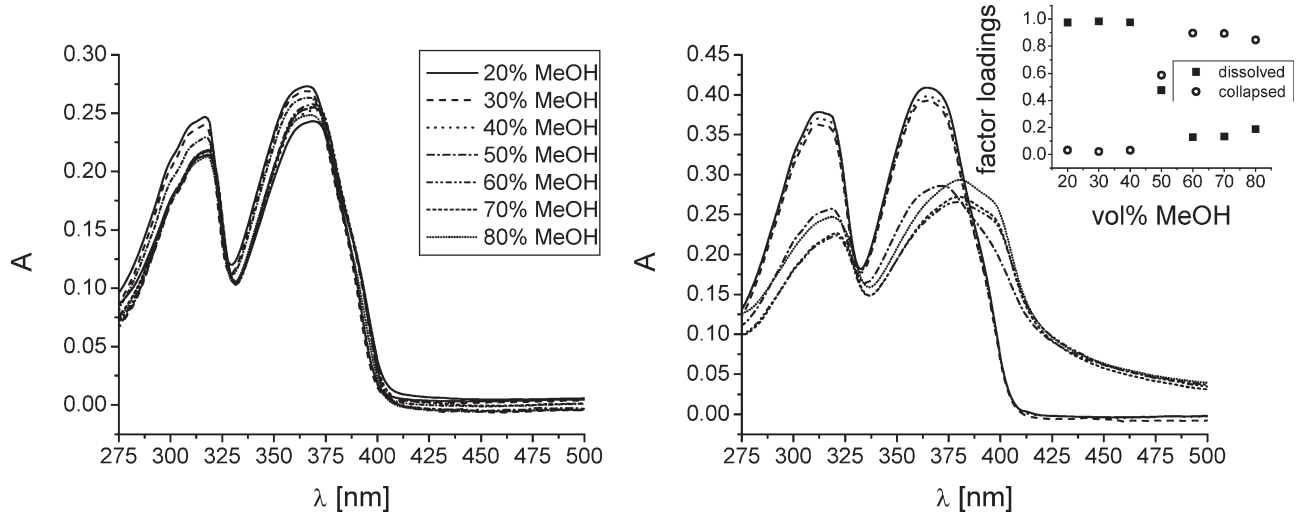

FIGURE 4 UV–vis absorption spectrum of **M2** (left) and **P2b** (right) in $CHCl_3$ at different MeOH concentrations. The inset shows the factor loadings of the factor analysis, for two species, contributing to the absorption spectra.

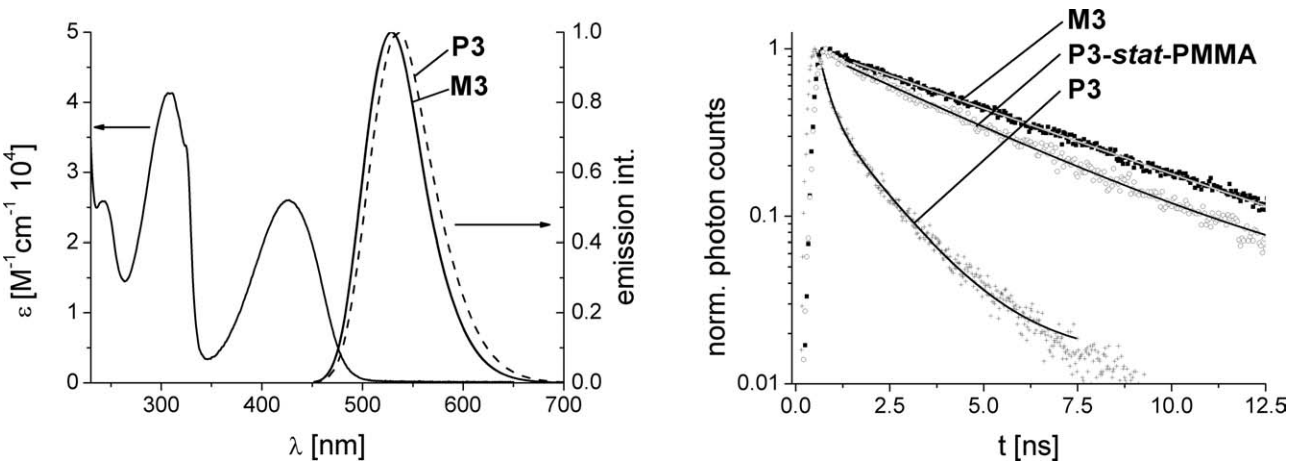

FIGURE 5 Steady-state extinction of **M3** and emission spectra of **M3** and **P3** (left), time-correlated single photon counting measurement in dichloromethane at 296 K (right). Solid lines represent the fitting curves.

The influence of the polymerization of **M2** and **M3** on the emission properties was additionally investigated by time-resolved measurements and measurements of the fluorescence quantum yields of polymerized and unpolymerized species. The results of these measurements are summarized in Table 3: comparing the quantum yields of **M3**, **P3-*stat*-PMMA**, and **P3**, one finds that the quantum yield is reduced by 20% when **M3** is polymerized to **P3-*stat*-PMMA** and is further reduced when **M3** is polymerized to homopolymer **P3**.

Accordingly, a shortening of the fluorescence lifetimes is observed after polymerization of **M3** (see Fig. 5, right). This indicates that polymerization of **M3** causes quenching of the fluorescence. As described by Farinha and Martinho,[49] quenching of emission in RAFT polymers can be caused by the RAFT end group. Furthermore, in polymers processes, such as singlet energy migration, chromophore diffusion, segmental rotation, and energy trapping by excimer-forming sites might play important roles in fluorescence quenching. For **P3**, the fluorescence quenching is stronger than that for **P3-*stat*-PMMA** because of the higher chromophore content leading to an enhanced interaction of the adjacent chromophores. These interactions result in an increased trapping efficiency. Furthermore, for **P3**, the emission decay is not single-exponential anymore (Fig. 5, right). This is often observed in polymers with high chromophore fractions.[50,51] In order to decipher the reason for the changed fluorescence decay times after polymerization, time-resolved anisotropy measurements were applied and used to test for energy migration in the polymers **P3-*stat*-PMMA** and **P3**. Generally, energy migration accelerates fluorescence depolarization.[52] Thus, a shortening in the anisotropy decay of **P3-*stat*-PMMA** and **P3** compared with **M3** could provide indications for energy migration within the polymers.

For time-resolved fluorescence anisotropy measurements, the trans axis of the polarizer on the emission side was set to vertical orientation while the polarization of the excitation light was set by a zero-order half-wave-plate perpendicular and parallel to the trans axis of the emission polarizer. This setup was chosen in order to avoid distortion of the intensity ratio between perpendicular and parallel intensities through the polarization sensitive imaging spectrograph. Before recording the fluorescence intensities with perpendicular and parallel polarized laser pulses, the sensitivity of the setup for perpendicular and parallel polarized light was tested (see Fig. 6, left). Therefore, scattered photons from a diluted scatterer irradiated with the used excitation pulses were detected with perpendicular and parallel orientation between the laser polarization and the trans axis of the Glan–Thompson polarizer placed in the emission channel. For perpendicular orientation, only 40 counts in the maximum were detected, in contrast, to more than 5,000 counts in the maximum for parallel orientation. Thus, the setup used for time-resolved fluorescence anisotropy measurements is highly sensitive for the polarization direction.

The anisotropy $r(t)$ was calculated using the measured intensities I_{vv} and I_{hv}: $r(t) = (I_{vv} - I_{hv})/(I_{vv} + 2I_{hv})$.

The experimental time-resolved anisotropies are shown in Figure 6, right: the decays were fitted by the single-exponential decay $r(t) = r_0 \exp[(t - t_0)/\theta] + r_\infty$, where r_0 is the initial anisotropy, t_0 is the excitation point in time, Θ is the anisotropy relaxation time, and r_∞ is the residual anisotropy. This decay function can successfully describe the anisotropy of the monomer and the polymers. Although the fit function is not rooted in a molecular modeling of the physical processes leading to fluorescence anisotropy decay, it delivers values for the anisotropy correlation time, which can be discussed qualitatively and used for mutual comparison of the different compounds (Table 4).

Comparing the values of the anisotropy fit constants in Table 4, it can be noted that for all compounds, the sum of r_0 and r_∞ is smaller than 0.4, which is the maximum value of anisotropy for randomly orientated fluorophores with parallel absorption and emission transition moments. When assuming randomly orientated fluorophores in solution, the initial anisotropy $r_0 + r_\infty$ is expected to be 0.4. Values below 0.4

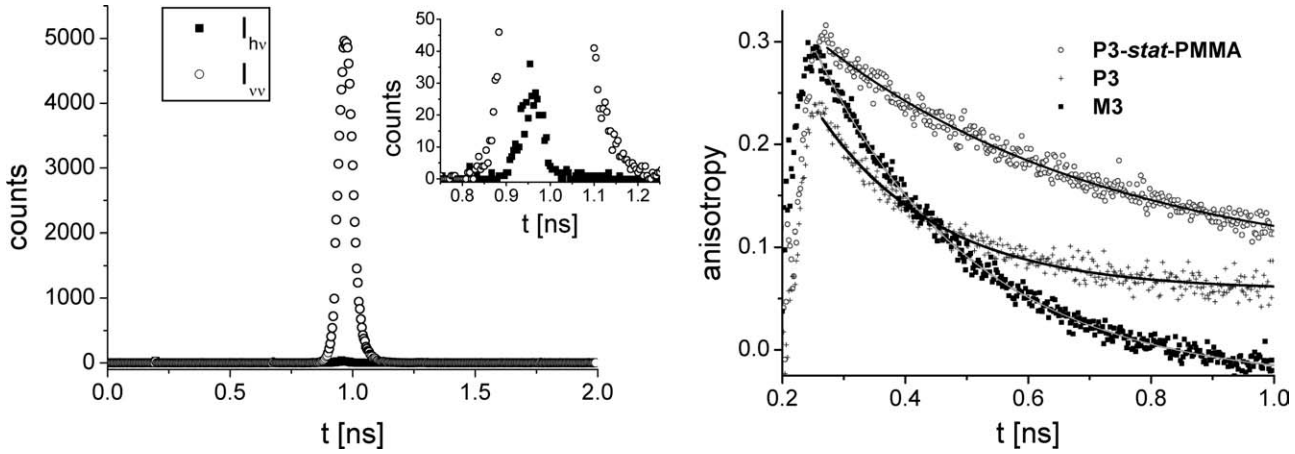

FIGURE 6 Sensitivity test of the setup for perpendicular and parallel polarized light (left). The inset shows a zoom-in into the region of interest. Fluorescence anisotropy decay in dichloromethane at RT (right). The anisotropy was calculated from $r(t) = (I_{vv} - I_{hv})/(I_{vv} + 2I_{hv})$. Solid lines represent the fit.

point to depolarizing effects, which are not fully time-resolved experimentally. For the polymer **P3**, the initial anisotropy, $r_0 + r_\infty$ is smaller than that of the monomer **M3**, indicating a fast depolarization process, which is not captured within the time resolution of the experiment. This process is apparently not observable for **P3-*stat*-PMMA**. The anisotropy relaxation time of **M3** (0.26 ns) is the time in which rotational diffusion takes place. For **M3**, rotational diffusion is the reason why the fluorescence becomes depolarized. In polymers like **P3** and **P3-*stat*-PMMA**, the fluorescence depolarization can be caused by energy transfer between individual fluorophores (homo energy transfer). In cooperation with rotational diffusion, one would hence expect a faster loss of the fluorescence anisotropy compared to the monomer **M3**.[52,53] This is the case, when considering the initial value $r_0 + r_\infty$ of the anisotropy for **P3**. The value of the initial anisotropy indicates fast fluorescence depolarization for the polymer **P3** which is not time resolved with the experimental setup in addition to the measurable anisotropy decay time of 0.19 ns.

In addition to the rapidly decaying anisotropy components, the polymer anisotropies exhibit long-lived non-zero components r_∞. These are most likely due to slower overall rotational motion of the polymer chains. The reduced relaxation time for **P3** compared to **P3-*stat*-PMMA** stems from conformational differences between the polymers, which lead to different volumes of the rotating molecule, and thus, different rotation correlation times. The number of repeating units is estimated to be 21 and 78 for **P3** and **P3-*stat*-PMMA**, respectively. In the latter polymer, 8 mol % of the repetiting units exhibit a chromophor in the side chain. These structural differences are one reason for the differences in the measured correlation times.

Finally, it can be stated that polymerization of **M3** reduces the lifetime and the emission quantum yield of the polymers compared to the single oligomer. The experimental data for the fluorescence anisotropy indicate energy migration within the polymer chain of **P3**, but further studies with improved temporal resolution need to detail the kinetics of the process.

A different photophysical behavior after polymerization was found for **M2**, **P2-*stat*-PMMA**, and **P2**: the emission quantum yield is increased when **M2** is polymerized to **P2-*stat*-PMMA**. For **P2**, the quantum yield is again reduced (Table 3). The fluorescence lifetimes of the oligomers in the polymers indicate the same type of behavior as the quantum yields. This means that in **P2-*stat*-PMMA** nonradiative decay rates are reduced most likely by environmental and structural changes upon polymerization. This was also observed for another **PMMA** polymer with fluorophores in the side chains.[28] Similar to **P2-*stat*-PMMA** and **P3**, the fluorescence decay changes from a mono-exponential decay for **P2-*stat*-PMMA** to a more complex decay for **P2**, the latter likely caused by increased interactions of adjacent chromophores because of the high molar fraction of chromophores (100%) in the polymer side chain.

As already discussed for **P3**, the non-mono-exponentially decay of the homopolymer emission and the weak fluorescence quantum yield of **P2** and **P3** indicate homo-energy transfer within the polymer, which becomes feasible by the close spatial arrangement of chromophores in the polymers.

In order to design a system capable of hetero-energy transfer, the statistical donor–acceptor copolymer **P2-*stat*-P3** was

TABLE 4 Fitting Parameter for the Anisotropy Decay: $r(t) = r_\infty + r_0 \exp(-t/\Theta)$

Sample	r_0	Θ (ns)	r_∞
M3	0.32	0.26	−0.03
P3-*stat*-PMMA	0.22	0.48	0.07
P3	0.17	0.19	0.06

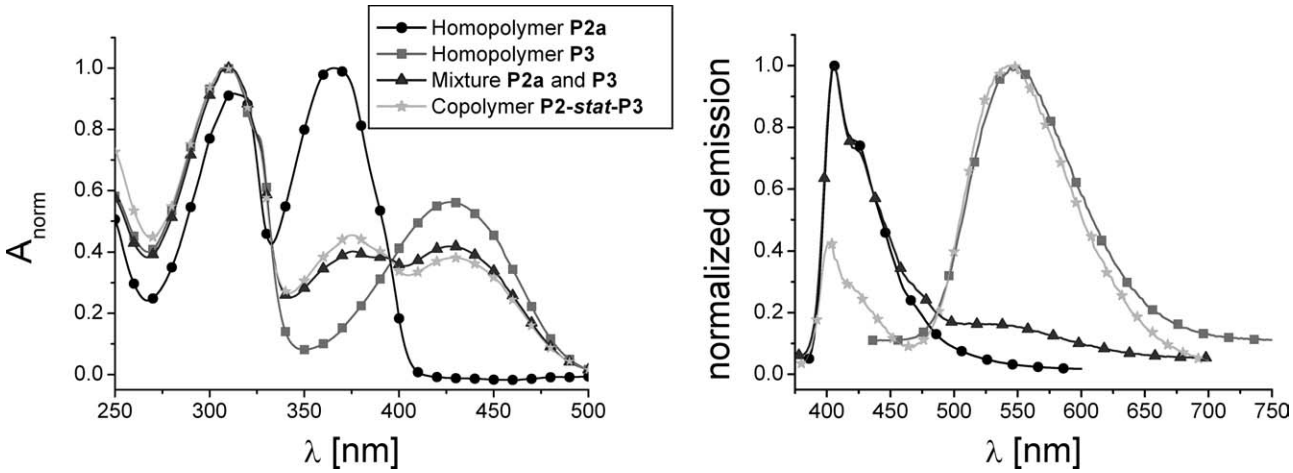

FIGURE 7 Comparison of UV–vis absorption (left) and emission spectra (right) of the homopolymers **P2a** (λ_{exc} = 375 nm) and **P3** (λ_{exc} = 429 nm), the copolymer **P2-*stat*-P3** (λ_{exc} = 375 nm), and its corresponding mixture of the homopolymers (λ_{exc} = 375 nm) in solution.

prepared. For a comparison, an analogous mixture of both homopolymers (30:70 **P2**:**P3**) was investigated via UV–vis spectroscopy. This was done for $CHCl_3$ solutions with increasing MeOH content (Supporting Information). In both cases, a similar behavior was observed, i.e., with increasing content of MeOH, lower absorbances and bathochromic shifts of the absorption bands are observed.

A hint towards energy transfer in the donor–acceptor copolymer (**P2-*stat*-P3**) is given in Figure 7. The absorption and emission spectra of both homopolymers, homopolymer mixture, and **P2-*stat*-P3** are displayed. The shape of the absorption spectra of **P2-*stat*-P3** and the homopolymer mixture is virtually identical, which leads to the conclusion that the mixture has the same composition as the statistical copolymer. The emission spectrum of the mixture shows that if the donor is excited exclusively, mainly donor emission is observed. The residual emission of the acceptor can be assigned to either weak donor–acceptor energy transfer or – more likely – to direct excitation of the acceptor units due to the small non-zero acceptor absorption coefficient at the excitation wavelength. In the case of the copolymer, primarily the acceptor fluorescence could be observed if the donor is excited. Hence, donor–acceptor energy transfer is observed with the donor emission overlapping with the acceptor absorption. Therefore, Förster energy transfer can occur, if the distance between the donor and acceptor is sufficiently small[54] as in the statistical copolymer (R_0 = 43 Å).

The absorption and emission behavior of the films (Fig. 8) differ from the behavior of the polymers in solution: generally, the shape of the absorption spectra of the films is virtually identical to the spectra in solution; however, the absorption maxima are shifted to longer wavelengths. Thus, the

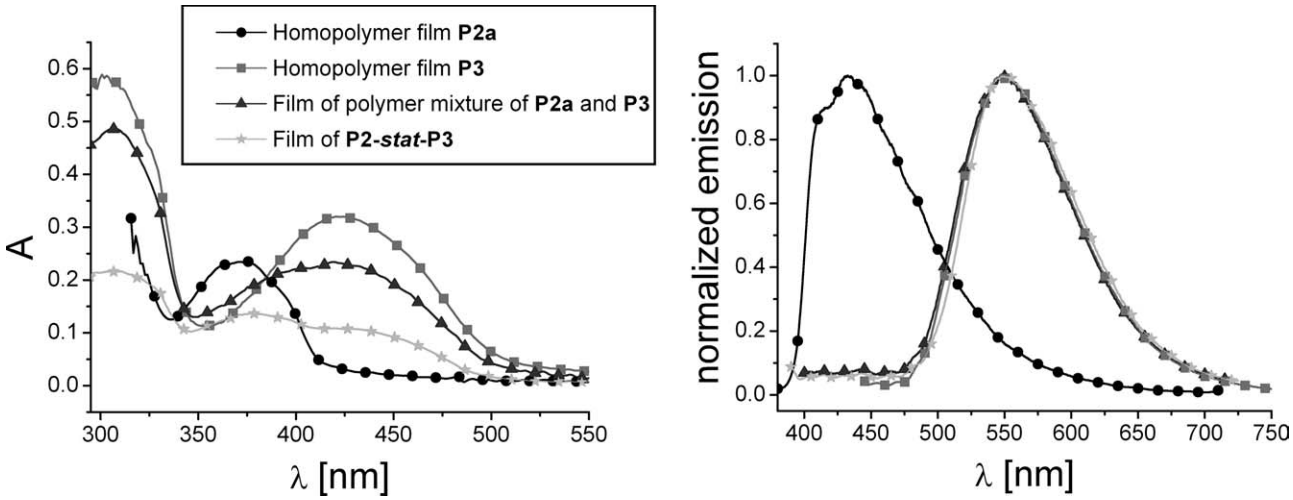

FIGURE 8 Comparison of UV–vis absorption (left) and emission spectra (right) of the homopolymer films **P2a** (λ_{exc} = 375 nm) and P3 (λ_{exc} = 429 nm), the copolymer film **P2-*stat*-P3** (λ_{exc} = 375 nm), and the corresponding film of the homopolymer mixture (λ_{exc} = 375 nm).

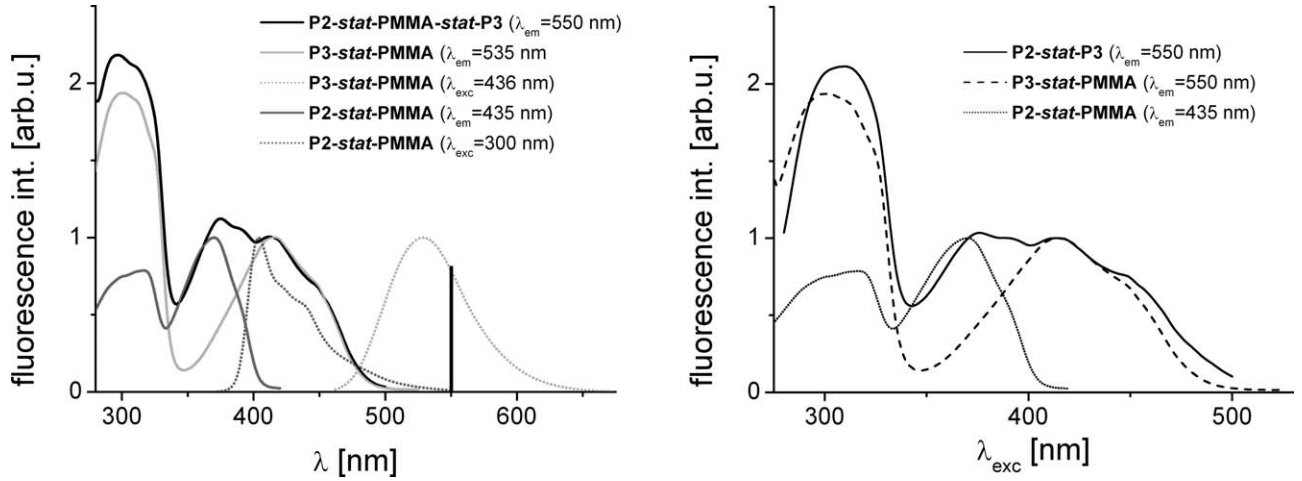

FIGURE 9 Emission and excitation spectra of **P2-*stat*-PMMA**, **P3-*stat*-PMMA**; and excitation spectrum of **P2-*stat*-PMMA-*stat*-P3** (left); and excitation spectra of **P2-*stat*-PMMA**, **P3-*stat*-PMMA**, and **P2-*stat*-P3** (right) in dichloromethane at 296 K.

emission of the homopolymer mixture as well as the **P2-*stat*-P3** shows energy transfer. This effect can be explained by the shorter distances between different polymer chains and a closer packing in the films. Presumably, energy transfer in solution only takes place between the oligomers of one chain due to low concentrations used in the UV–vis spectroscopy experiments. In contrast, the intermolecular distances between donor and acceptor units in the optical active polymer parts are small enough to allow for quantitative energy transfer.

A further illustration of RET is given in Fig. 9, where fluorescence excitation spectra of the donor, acceptor, and donor–acceptor polymers are depicted together with donor and acceptor emission spectra: the donor and acceptor fluorescence excitation spectra are clearly separated from each other. However, when the acceptor excitation in the donor–acceptor polymer is recorded at 550 nm, an additional excitation band is observed, which stems from excited donor molecules which have transferred their excitation energy to acceptor molecules.

For both donor–acceptor polymers **P2-*stat*-PMMA-*stat*-P3** and **P2-*stat*-P3**, fluorescence excitation spectra could be measured. This could give rise to the assumption that the two donor–acceptor systems reveal similar photophysical properties. However, this is contradicted by the steady-state emission spectra of the donor–acceptor polymer **P2-*stat*-PMMA-*stat*-P3** in Fig. 10. The shape of the donor fluorescence from the donor–acceptor polymer **P2-*stat*-PMMA-*stat*-P3** differs from the emission shape of **P2-*stat*-P3** (Fig. 10). The blue donor emission from **P2-*stat*-PMMA-*stat*-P3** at 400 nm has dropped in intensity compared to the donor emission at 435 nm (Fig. 10, left).

This behavior is not observed for **P2-*stat*-P3** (Fig. 7, right) and not for **M2** and has to be investigated more in detail: such a dip in the emission spectra of **P2-*stat*-PMMA-*stat*-P3** could indicate reabsorption of emitted photons. But, for our polymers, reabsorption caused by high concentration is not detected because after dilution the emission spectra are nearly unchanged, what is obvious from Figure 10, right.

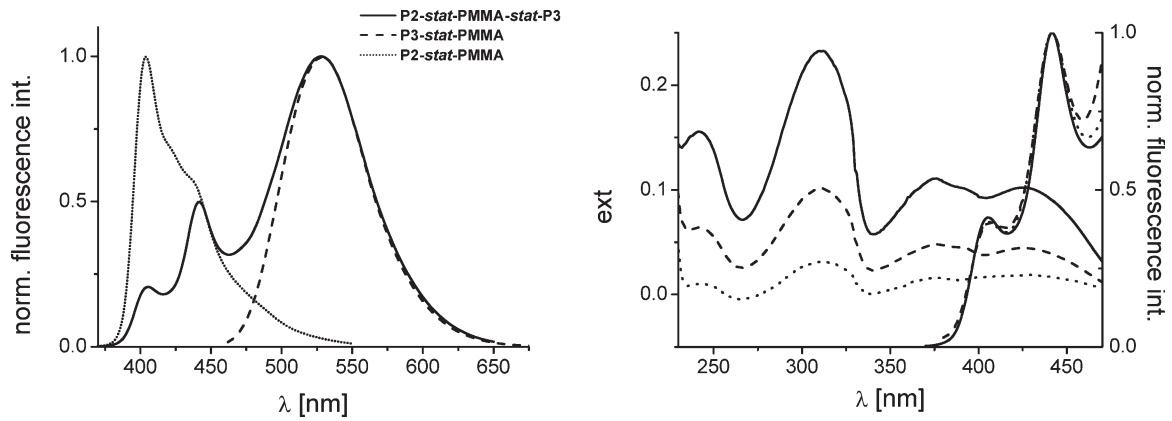

FIGURE 10 Emission of **P2-*stat*-PMMA**, **P2-*stat*-PMMA-*stat*-P3**, $\lambda_{exc} = 375$ nm and **P3-*stat*-PMMA**, $\lambda_{exc} = 430$ nm (left). Absorbance and emission of **P2-*stat*-PMMA-*stat*-P3** in dichloromethane at 296 K after dilution, $\lambda_{exc} = 375$ nm (right).

EXPERIMENTAL

Material and General Experimental Details

All chemicals used were purchased from Biosolve, Fluka, Aldrich, Acros Organics as well as Alfa Aesar and were used without further purification unless otherwise specified. The solvents were dried and distilled according to standard procedures. Preparative size exclusion chromatography was performed on Bio-Rad S-X3 beads (size exclusion limit 2,000 g/mol), swollen in toluene.

Instrumentation

1D (^{1}H, ^{13}C) and 2D (HSQC) NMR spectra were recorded on a Bruker AC 300 (300 MHz) and a Bruker AC 250 (250 MHz) at 298 K. Chemical shifts are reported in parts per million (ppm, δ scale) relative to the residual signal of the deuterated solvent. Coupling constants are given in hertz. UV–vis absorption and PL emission spectra were recorded on an Analytik Jena SPECORD 250 and a Jasco FP-6500 spectrometer, respectively, at 298 K. Absolute PL quantum yields were evaluated at 298 K using a Hamamatsu Photonic Multi-Channel Analyzer C 10027. For these techniques, dilute solutions (10^{-6}–10^{-5} M, 1 cm quartz cuvette) in chloroform were used. As reference, a quartz cuvette filled with pristine solvent was used. Matrix-assisted laser desorption/ionization time-of-flight mass spectra (MALDI-TOF MS) were obtained using an Ultraflex III TOF/TOF mass spectrometer with dithranol, *trans*-2-[3-(4-*tert*-butylphenyl)-2-methyl-2-propenylidene]malononitrile (DCTB), or terthiophene as matrix in reflector as well as linear mode, respectively. The instrument was calibrated prior to each measurement with an external PMMA standard from PSS Polymer Standards Services GmbH (Mainz, Germany). Elemental analysis was performed on a CHN-932 Automat Leco instrument. Size exclusion chromatograms were recorded on a SEC Shimadzu SCL-10A system controller, LC-10AD pump, RID-10A refractive index detector, and PSS SDV pre/lin S column at 50 °C (eluent: chloroform:triethylamine:*iso*-propanol 94:4:2; flow rate of 1 mL/min) using linear PS or PMMA standards. Spin coating was performed at various spin speeds and accelerations with a spin coater from Laurell Technologies Corporation (North Wales). The spin coating time was set to 30 s, and the experiments were performed at room temperature (RT). Surface topography was measured by an optical interferometric profiler Wyko NT9100 (Veeco, Mannheim, Germany). The profiler was also used to determine the thicknesses of the films. For this purpose, each film was scratched with a scalpel in a controlled manner. At five different positions of the film, the depth of the scratch was measured with the optical profiler. These positions are the center of the film and the four edges where the scratch is located. A UV–vis/fluorescence plate reader from Analytik Jena (FLASHScan 530, Jena, Germany) was used to measure the UV–vis absorption spectra of the films. For the microscope slides, an adapter was used. The measurements were referenced to air. Fluorescence of the films was measured with a modified Hitachi F-4500. AFM measurements were performed in tapping mode either with a NTegra Aura (NT-MDT, Moscow, Russia) or using a Nanoscope IIIa Multimode (Digital Instruments, Veeco, Santa Barbara, CA) with commercially available TiN-coated cantilevers (NSC35, MicroMash). Sedimentation velocity experiments were performed using a Beckman XLI analytical ultracentrifuge (ProteomeLab XLI Protein Characterization System) with interference optics and Al-double-sector cells of optical path 12 mm. Rotor speed was 40,000 or 45,000 rpm at 20 °C. The thermogravimetric analysis (TGA) analysis was performed on a Netzsch TG 209 F1 (heating rate: 10 K min^{-1}; T_d is given at 5% weight loss), and the differential scanning calorimetry (DSC) was measured on a DSC 204 F1 Phoenix by Netzsch under a nitrogen atmosphere in a temperature range from −100 to 200 °C with a heating rate of 20 K min^{-1} (T_g values are reported as onset values from the second heating run).

Steady-state emission measurements were performed as already described in previous publications.[38] Briefly, emission quantum yields were measured by comparing the corrected emission intensities of the solvents with the fluorescence intensity of the standard quinine sulfate with a quantum yield of 55%. The excitation wavelength was set to the most red-shifted absorption maximum, whereby the extinction maximum was kept below 0.05.

The fluorescence decay curves were obtained by a Hamamatsu streakscope C4334 in time-correlated single photon counting modus under magic angle configuration. Triggering was performed by the Hamamatsu trigger unit C4792-01. After excitation with a frequency-tripled Ti-sapphire laser (Tsunami, Newport Spectra-Physics GmbH), i.e., $\lambda_{ex} = 290$ nm, in perpendicular direction, the fluorescence emission wavelength was separated by a Chromex 250IS imaging spectrograph. The repetition rate of the laser was adjusted to 0.8 MHz by a pulse selector (model 3980, Newport Spectra-Physics GmbH). All measurements were performed at concentrations below 10^{-6} M.

General Procedure for the RAFT Polymerization

The desired amounts of the monomers (for detailed information on the synthesis and characterization, see Supporting Information) were transferred into the reaction vial (5 mL reaction vessel) and dissolved in toluene. Thereafter, the calculated volumes of stock solutions of CBDB in toluene and AIBN in toluene were added. The ratio of [CBDB]:[AIBN] was always 4:1. Before closing the vial, the reaction solution was purged with a flow of argon for 30 min. Subsequently, the reaction was performed in an oil bath at 70 °C overnight (see Table 1 for the exact reaction times and [M]/[CBDB] ratios). The obtained polymers were purified by precipitation into cold ethanol. The polymers were dried under reduced pressure at RT. In contrast, THF was used as solvent instead of toluene for the polymerization of **M3** or the copolymerizations, respectively. Before degassing, the solution was heated to 40 °C and filtered hot to dissolve as much monomer as possible. Purification by column chromatography using a BioBeads S-X3 column (solvent toluene, exclusion limit

2,000 g/mol) and a second precipitation into cold ethanol was required for these samples.

Homopolymer P1

^{1}H NMR ($CDCl_3$, 300 MHz): δ = 0.91 (b, CH_3, backbone and alkoxy chain), 1.1 to 1.6 (b, CH_2 backbone and alkoxy chain), 2.30 (b, enclosed H_2O), 3.89 (OCH_2), 6.74 (b, ArH), 7.01 (b, ArH), 7.40 (b, ArH) ppm. EA: C: 78.19%, H: 7.15%, N: 0.17%, S: 0.88% (**P1a**); C: 77.93%, H: 6.91%, N: 0.15%, S: 0% (**P1b**); C: 78.24%, H: 6.96%, N: 0,14%, S: 0% (**P1c**); C: 78.52%, H: 6.74%, N: 0.31%, S: 0.43% (**P1d**); C: 78.59%, H: 6.84%, N: 0.14%, S: 0% (**P1e**). SEC ($CHCl_3$, PS standard): M_n = 17,000 g/mol (**P1a**), 24,000 g/mol (**P1b**), 33,100 g/mol (**P1c**), 8,800 g/mol (**P1d**), 16,400 g/mol (**P1e**); M_w = 21,900 g/mol (**P1a**), 32,900 g/mol (**P1b**), 61,200 g/mol (**P1c**), 11,000 g/mol (**P1d**), 21,200 g/mol (**P1e**); PDI = 1.29 (**P1a**), 1.37 (**P1b**), 1.85 (**P1c**), 1.25 (**P1d**), 1.29 (**P1e**). DSC: T_g = 150 °C (**P1a**), 170 °C (**P1b**), 178 °C (**P1c**), 123 °C (**P1d**), 169 °C (**P1e**). TGA: T_d = 320 °C (**P1a**), 340 °C (**P1b**), 320 °C (**P1c**), 290 °C (**P1d**), 310 °C (**P1e**). AUC: M_{AUC} = 58,000 g/mol (**P1b**); 14,000 g/mol (**P1d**).

Homopolymer P2

^{1}H NMR ($CDCl_3$, 300 MHz): δ = 0.75, 0.84 (b, CH_3, backbone and alkoxy chain), 1.1 to 1.8 (b, CH_2 backbone and alkoxy chain), 3.86 (b, OCH_2), 6.74, 6.84, 7.01, 7.35 (b, ArH) ppm. EA: C: 76.99%, H: 8.00%, N: 0.17%, S: 0% (**P2a**); C: 78.61%, H: 8.14%, N: 0.16%, S: 0% (**P2b**). SEC ($CHCl_3$, PS standard): M_n = 13,600 g/mol (**P2a**), 14,400 g/mol (**P2b**); M_w = 16,300 g/mol (**P2a**), 17,900 g/mol (**P2b**); PDI = 1.20 (**P2a**), 1.24 (**P2b**). DSC: no T_g or T_m observed. TGA: T_d = 370 °C (**P2a**), 360 °C (**P2b**).

Homopolymer P3

^{1}H NMR ($CDCl_3$, 300 MHz): δ = 0.92 (b, CH_3, backbone and alkoxy chain), 1.2 to 1.9 (b, CH_2 backbone and alkoxy chain), 3.93 (b, OCH_2), 6.80 (b, ArH), 7.10 (b, ArH), 7.51 (b, ArH) ppm. EA: C: 72.73%, H: 5.08%, N: 5.25%, S: 6.09%. SEC ($CHCl_3$, PS standard): M_n = 11,100 g/mol; M_w = 13,300 g/mol; PDI = 1.20. DSC: no T_g or T_m observed. TGA: T_d = 408 °C.

Statistical Donor/Acceptor-Copolymer P2-*stat*-P3

^{1}H NMR ($CDCl_3$, 300 MHz): δ = 0.83, 0.92 (b, CH_3, backbone and alkoxy chains), 1.1 to 1.9 (b, CH_2, backbone and alkoxy chains), 3.94 (OCH_2), 6.81, 6.92, 7.10, and 7.52 (b, ArH) ppm. EA: C: 74.95%, H: 6.10%, N: 3.37%, S: 4.03%. SEC ($CHCl_3$, PS standard): M_n = 9,300 g/mol; M_w = 10,800 g/mol, PDI = 1.16. DSC: no T_g or T_m observed. TGA: T_d = 402 °C.

Donor Containing PMMA P2-*stat*-PMMA

^{1}H NMR ($CDCl_3$, 300 MHz): δ = 0.89, 1.02, (b, CH_3, backbone and alkoxy chains) 1.35, 1.59, 1.82 (b, CH_2, backbone and alkoxy chains), 3.60 (b, OCH_3 PMMA), 4.00 (b, OCH_2), 6.85, 6.87, 6.99, 7.09, 7.44, 7.47, 7.52, and 7.55 (b, ArH) ppm. EA: C: 69.87%, H: 8.24%, N: 0.15%, S: 0.00%. SEC ($CHCl_3$, PS standard): M_n = 14,600 g/mol; M_w = 18,100 g/mol, PDI = 1.24. DSC: T_g = 87 °C. TGA: T_d = 210 °C.

Acceptor Containing PMMA P3-*stat*-PMMA

^{1}H NMR (CD_2Cl_2, 300 MHz): δ = 0.84, 1.02, 1.25, 1.38, 1.50, 1.59, 1.83, and 1.91 (b, CH_2 and CH_3, backbone and alkoxy chains), 3.64 (b, OCH_3 PMMA), 4.03 (b, OCH_2), 6.95, 6.97, 7.21, 7.59, 7.62, 7.70, 7.81, and 7.91 (b, ArH) ppm. EA: C: 64.95%, H: 7.68%, N: 1.37%, S: 1.52%. SEC ($CHCl_3$, PS standard): M_n = 10,500 g/mol; M_w = 12,300 g/mol, PDI = 1.17. DSC: T_g = 47 °C. TGA: T_d = 210 °C.

Statistical Donor/Acceptor Containing PMMA P2-*stat*-PMMA-*stat*-P3

^{1}H NMR ($CDCl_3$, 300 MHz): δ = 0.89, 1.05, 1.35, 1.47, 1.79, and 2.07 (b, CH_2 and CH_3, backbone and alkoxy chains), 3.61 (b, OCH_3 PMMA), 3.97 (b, OCH_2), 6.87, 6.98, 7.12, 7.44, 7.57, and 7.67 (b, ArH) ppm. EA: C: 70.49%, H: 6.82%, N: 2.53%, S: 2.78%. SEC ($CHCl_3$, PS standard): M_n = 10,800 g/mol; M_w = 14,000 g/mol, PDI = 1.30. DSC: T_g = 38 °C. TGA: T_d = 255 °C.

CONCLUSIONS

In summary, the synthesis and characterization of homo- and statistical copolymers, which contain monodisperse conjugated oligomers (OPEs) as side chains were described, using the RAFT polymerization technique. The polymers combine the well-defined and adjustable optical properties of the OPE systems with typical polymer properties (e.g., film formation) of the polymer backbone; the length and composition of the polymer can be controlled by the RAFT polymerization process. Moreover, the close spatial arrangement of the conjugated subunits enhanced the interaction between the OPEs and changed the optical properties, compared with the nonpolymerized oligomer.

For this purpose, a series of three different OPEs, containing a polymerizable methacrylate function, were synthesized by *Sonogashira* cross-coupling reactions, varying the length of the oligomer (donor dimer and trimer; **M1** and **M2**) as well as the optoelectronic properties (donor and acceptor trimer; **M2** and **M3**). After the RAFT polymerization, the polymers were characterized by ^{1}H NMR spectroscopy, SEC, and MALDI-TOF mass spectrometry. In addition, further information about the absolute molar masses of the polymers (**P1c**, **P1d**, and **P1e**) was obtained from AUC; the latter results indicate that the molar masses obtained by SEC are underestimated by a factor of 1.4–2.

Besides these homopolymers (**P1**–**P3**), also a random copolymer was synthesized using **M2** and **M3**, which contains "donor" as well as "acceptor" units. In addition, the donor trimer as well as the acceptor trimer content along the polymer chain was lowered by copolymerization with MMA (**P2-*stat*-PMMA**, **P3-*stat*-PMMA**, and **P2-*stat*-PMMA-*stat*-P3**).

The optical properties of the monomers and polymers were investigated in solution as well as in thin films. All polymers revealed an identical absorption in solution compared with the corresponding monomer unit. Furthermore, interactions between the oligomers in the homopolmer chains were induced by an increasing MeOH content in the solvent, which could be demonstrated via UV–vis absorption spectroscopy. A hint toward homo energy transfer between

oligomers in the homopolymer **P3** is given by time-resolved fluorescence anisotropy measurements. The increased oligomer fraction in polymer **P3** causes smaller distances between the oligomers than in **P3-*stat*-PMMA** allowing for higher rates of energy transfer. For the statistical donor–acceptor copolymers, a dual fluorescence was observed and the acceptor fluorescence exhibits clearly contributions from excitation through donor molecules. This suggests the conclusion that an energy transfer occurred.[54] Film formation, which leads to higher spatial aggregation of the chromophores, caused higher interactions of the π-conjugated oligomers. Having this information in hand, the described system can be potentially applied as antenna system to mimic light-harvesting photosynthetic proteins in plants.

ACKNOWLEDGMENTS

The authors thank the Thüringer Ministerium für Bildung, Wissenschaft und Kultur (Grant No. B 514-09049: Photo-Mic) as well as the Dutch Polymer Institute (DPI, technology area HTE). U. S. Schubert, B. Dietzek, and J. Popp acknowledge financial support of the Fonds der Chemischen Industrie.

REFERENCES AND NOTES

1 Liu, P.; Liu, W. M.; Xue, Q. J. *J. Macromol. Sci. Pure Appl. Chem.* **2004,** *A41*, 1001–1010.

2 Plank, J.; Dai, Z. M.; Zouaoui, N. *J. Phys. Chem. Solids* **2008,** *69*, 1048–1051.

3 Kirby, G. H.; Harris, D. J.; Li, Q.; Lewis, J. A. *J. Am. Ceram. Soc.* **2004,** *87*, 181–186.

4 Rzayev, J. *Macromolecules* **2009,** *42*, 2135–2141.

5 Hyun, J. H.; Ma, H. W.; Zhang, Z. P.; Beebe, T. P.; Chilkoti, A. *Adv. Mater.* **2003,** *15*, 576–579.

6 Hyun, J. H.; Ma, H. W.; Banerjee, P.; Cole, J.; Gonsalves, K.; Chilkoti, A. *Langmuir* **2002,** *18*, 2975–2979.

7 Banerjee, P.; Irvine, D. J.; Mayes, A. M.; Griffith, L. G. *J. Biomed. Mater. Res.* **2000,** *50*, 331–339.

8 Ying, Z.; Costantini, N.; Mierzwa, M.; Pakula, T.; Neugebauer, D.; Matyjaszewski, K. *Polymer* **2004,** *45*, 6333–6339.

9 Pakula, T.; Zhang, Y.; Matyjaszewski, K.; Lee, H. I.; Boerner, H.; Qin, S. H.; Berry, G. C. *Polymer* **2006,** *47*, 7198–7206.

10 Huang, X. Y.; Feng, C.; Li, Y. J.; Yang, D.; Hu, J. H.; Zhang, X. H. *Chem. Soc. Rev.* **2011,** *40*, 1282–1295.

11 Gil, E. S.; Hudson, S. M. *Prog. Polym. Sci.* **2004,** *29*, 1173–1222.

12 Tsvetanov, C. B.; Dimitrov, I.; Trzebicka, B.; Muller, A. H. E.; Dworak, A. *Prog. Polym. Sci.* **2007,** *32*, 1275–1343.

13 Weber, C.; Becer, C. R.; Guenther, W.; Hoogenboom, R.; Schubert, U. S. *Macromolecules* **2010,** *43*, 160–167.

14 Pavlov, G. M.; Breul, A. M.; Hager, M. D.; Schubert, U. S. *Macromol. Chem. Phys.* **2012**. DOI: 10.1002/macp.201100653.

15 Shirota, Y. *J. Mater. Chem.* **2000,** *10*, 1–25.

16 Segura, J. L.; Martin, N. *J. Mater. Chem.* **2000,** *10*, 2403–2435.

17 Shirota, Y.; Nogami, T.; Kakuta, T.; Saito, H. *Synth. Met.* **1991,** *41*, 1169–1172.

18 Jeon, I. R.; Noma, N.; Shirota, Y. *Bull. Chem. Soc. Jpn* **1992,** *65*, 1062–1066.

19 Obi, M.; Morino, S.; Ichimura, K. *Chem. Mater.* **1999,** *11*, 1293–1301.

20 Zhao, C. C.; Zhang, Y.; Pan, S. L.; Rothberg, L.; Ng, M. K. *Macromolecules* **2007,** *40*, 1816–1823.

21 Sommer, M.; Huttner, S.; Steiner, U.; Thelakkat, M. *Appl. Phys. Lett.* **2009,** *95*, 183308.

22 Sommer, M.; Huttner, S.; Wunder, S.; Thelakkat, M. *Adv. Mater.* **2008,** *20*, 2523–2527.

23 Sommer, M.; Lang, A. S.; Thelakkat, M. *Angew. Chem. Int. Ed. Engl.* **2008,** *47*, 7901–7904.

24 Lindner, S. M.; Huttner, S.; Chiche, A.; Thelakkat, M.; Krausch, G. *Angew. Chem. Int. Ed. Engl.* **2006,** *45*, 3364–3368.

25 Sivula, K.; Ball, Z. T.; Watanabe, N.; Frechet, J. M. *J. Adv. Mater.* **2006,** *18*, 206–210.

26 Frechet, J. M. J.; Serin, J.; Schultze, X.; Adronov, A. *Macromolecules* **2002,** *35*, 5396–5404.

27 Schultze, X.; Serin, J.; Adronov, A.; Frechet, J. M. *J. Chem. Commun.* **2001,** 1160–1161.

28 Happ, B.; Schaefer, J.; Menzel, R.; Hager, M. D.; Winter, A.; Popp, J.; Beckert, R.; Dietzek, B.; Schubert, U. S. *Macromolecules* **2011,** *44*, 6277–6287.

29 Pizzoferrato, R.; Berliocchi, M.; Di Carlo, A.; Lugli, P.; Venanzi, M.; Micozzi, A.; Ricci, A.; Lo Sterzo, C. *Macromolecules* **2003,** *36*, 2215–2223.

30 Weder, C.; Blankenburg, L.; Bunz, U. H. F.; Klemm, E.; Moore, J. S.; Pautzsch, T.; Ray, C. R.; Swager, T. M.; Voskerician, G.; Yamaguchi, I.; Yamamoto, T.; Yasada, T.; Zheng, J. *Adv. Polym. Sci.* **2005,** *177*, 1–50.

31 Barner-Kowollik, C.; Buback, M.; Charleux, B.; Coote, M. L.; Drache, M.; Fukuda, T.; Goto, A.; Klumperman, B.; Lowe, A. B.; Mcleary, J. B.; Moad, G.; Monteiro, M. J.; Sanderson, R. D.; Tonge, M. P.; Vana, P. *J. Polym. Sci. Part A: Polym. Chem.* **2006,** *44*, 5809–5831.

32 Tour, J. M. *Chem. Rev.* **1996,** *96*, 537–553.

33 Tschierlei, S.; Karnahl, M.; Presselt, M.; Dietzek, B.; Guthmuller, J.; Gonzalez, L.; Schmitt, M.; Rau, S.; Popp, J. *Angew. Chem. Int. Ed. Engl.* **2010,** *49*, 3981–3984.

34 Tschierlei, S.; Presselt, M.; Kuhnt, C.; Yartsev, A.; Pascher, T.; Sundstroem, V.; Karnahl, M.; Schwalbe, M.; Schaefer, B.; Rau, S.; Schmitt, M.; Dietzek, B.; Popp, J. *Chem. Eur. J.* **2009,** *15*, 7678–7688.

35 Kuhnt, C.; Karnahl, M.; Schmitt, M.; Rau, S.; Dietzek, B.; Popp, J. *Chem. Commun.* **2011,** *47*, 3820–3821.

36 Karnahl, M.; Kuhnt, C.; Ma, F.; Yartsev, A.; Schmitt, M.; Dietzek, B.; Rau, S.; Popp, J. *ChemPhysChem* **2011,** *12*, 2101–2109.

37 Holzwarth, A. Molecular to Global Photosynthesis; Imperial College Press: London, UK, **2004.**

38 Schaefer, J.; Menzel, R.; Weiss, D.; Dietzek, B.; Beckert, R.; Popp, J. *J. Lumin.* **2011,** *131*, 1149–1153.

39 Fijten, M. W. M.; Paulus, R. M.; Schubert, U. S. *J. Polym. Sci. Part A: Polym. Chem.* **2005,** *43*, 3831–3839.

40 Sessions, L. B.; Miinea, L. A.; Ericson, K. D.; Glueck, D. S.; Grubbs, R. B. *Macromolecules* **2005,** *38*, 2116–2121.

41 Quemener, D.; Le Hellaye, M.; Bissett, C.; Davis, T. P.; Barner-Kowollik, C.; Stenzel, M. H. *J. Polym. Sci. Part A: Polym. Chem.* **2008,** *46*, 155–173.

42 Zhao, H. Y.; Zhang, X. W.; Lian, X. M.; Liu, L.; Zhang, J. *Macromolecules* **2008,** *41*, 7863–7869.

43 Bouchekif, E.; Narain, R. *J. Phys. Chem. B* **2007,** *111*, 11120–11126.

44 Bunz, U. H. F. *Chem. Rev.* **2000,** *100*, 1605–1644.

45 Mizoshita, N.; Goto, Y.; Tani, T.; Inagaki, S. *Adv. Funct. Mater.* **2008,** *18*, 3699–3705.

46 Bao, C. Y.; Lu, R.; Jin, M.; Xue, P. C.; Tan, C. H.; Xu, T. H.; Liu, G. F.; Zhao, Y. Y. *Chem. Eur. J.* **2006,** *12*, 3287–3294.

47 Marcelja, S. *J. Chem. Phys.* **1974,** *60*, 3599–3604.

48 Dennler, G.; Scharber, M. C.; Brabec, C. *J. Adv. Mater.* **2009,** *21*, 1323–1338.

49 Farinha, J. P. S.; Martinho, J. M. G. *J. Phys. Chem. C* **2008,** *112*, 10591–10601.

50 Ghiggino, K. P.; Smith, T. A. *Prog. React. Kinet.* **1993,** *18*, 375–436.

51 Fredrickson, G. H.; Frank, C. W. *Macromolecules* **1983,** *16*, 572–577.

52 Johnson, J. M.; Chen, R.; Chen, X. Y.; Moskun, A. C.; Zhang, X.; Hogen-Eseh, T. E.; Bradforth, S. E. *J. Phys. Chem. B* **2008,** *112*, 16367–16381.

53 Smith, T. A.; Ghiggino, K. P. *Polym. Int.* **2006,** *55*, 772–779.

54 Sapsford, K. E.; Berti, L.; Medintz, I. L. *Angew. Chem. Int. Ed. Engl.* **2006,** *45*, 4562–4588.